Available online at www.sciencedirect.com

ScienceDirect

Geochimica et Cosmochimica Acta 255 (2019) 144–162

Geochimica et Cosmochimica Acta

www.elsevier.com/locate/gca

Oxygen isotopes in titanite and apatite, and their potential for crustal evolution research

E. Bruand [a,b,*], C. Storey [b], M. Fowler [b], E. Heilimo [c], EIMF [d]

[a] Laboratoire Magmas et Volcans Campus universitaire des Cézeaux, 6 avenue Blaise Pascal, TSA 60026 – CS 60026, 63178 Aubiere Cedex, France

[b] School of Earth and Environmental Sciences, University of Portsmouth, PO1 3QL, United Kingdom

[c] Geological Survey of Finland, P.O. Box 1237, FI-70211 Kuopio, Finland

[d] School of Geosciences, University of Edinburgh, West Mains Road, Edinburgh EH93JW, United Kingdom

Received 1 October 2018; accepted in revised form 1 April 2019; available online 16 April 2019

Abstract

Oxygen isotope analysis of zircon, often combined with geochronology and Hf isotope analysis, has been pivotal in understanding the evolution of continental crust. In this contribution, we expand the use of underexplored accessory phases (titanite and apatite) by demonstrating that their oxygen isotope systems can be robust, and by developing geochemical indicators involving O isotopes and trace element concentrations to better constrain magma petrogenesis. These minerals have the advantage over zircon of being present in less evolved magmas and being more responsive to igneous processes and crustal metamorphism. We present new data on titanite, apatite and zircon from carefully-selected granitoids through geological time: the Phanerozoic high Ba-Sr granites (Caledonian province, Scotland), Archean sanukitoids (Karelia province, Finland) and a Neoproterozoic basalt-andesite-dacite-rhyolite suite (BADR; Guernsey, Channel Island). We demonstrate: (i) that $\delta^{18}O$ values of the studied accessory minerals are not affected by crystal fractionation, (ii) a strong correlation between $\delta^{18}O$ in all three accessory minerals, showing that apatite and titanite can faithfully record the magmatic $\delta^{18}O$; (iii) that these accessory minerals can also record metamorphic and/or fluid circulation events during the syn- to post-magmatic history of granitoids.

Keywords: Oxygen isotopes; apatite; titanite; granitoids; crustal evolution

1. INTRODUCTION

By way of U-Pb dates and Hf-O isotopes in particular, zircon ($ZrSiO_4$) has provided evidence of crust formation processes even into the Hadean (4.4 Ga; e.g. Wilde et al., 2001; Bell et al., 2011) and plausible constraints on continental crust growth (Kemp et al., 2007). Recent high spatial-resolution in-situ radiogenic and stable isotope zircon datasets have greatly improved our understanding of crustal growth rates and mechanisms, especially when sedimentary and igneous zircon records are linked (e.g. Belousova et al., 2010; Dhuime et al., 2012). However, despite the impressive amount of zircon data now available, our knowledge is restricted to the information offered by the limited number of elements present in zircon (mainly HREE, U, Pb, Th and Hf). Although a few studies (Belousova et al., 2006; Grimes et al., 2015) have defined general discrimination diagrams using trace elements in zircon (for petrogenetic modelling and tectono-magmatic settings), its composition is generally not sensitive enough to record evolving magmatic conditions or to allow precise

* Corresponding author at: Laboratoire Magmas et Volcans, Campus universitaire des Cézeaux, 6 avenue Blaise Pascal, TSA 60026 – CS 60026, 63178 Aubiere Cedex, Finland.

E-mail address: emilie.bruand@uca.fr (E. Bruand).

https://doi.org/10.1016/j.gca.2019.04.002

0016-7037/

source attribution (e.g. Hoskin and Ireland, 2000; Hoskin and Schaltegger, 2003).

Unlike zircon, titanite and apatite are common minerals in mafic as well as felsic compositions, and they incorporate a larger range of detectable elements that are sensitive to melt evolution (LREE-MREE, Sr, Pb, Mn, halogens; Prowatke and Klemme 2006a; Gregory et al., 2009; Miles et al., 2014). Experimental work (Prowatke and Klemme; 2005; 2006a, 2006b; Stepanov et al., 2012; Li and Hermann 2017) has better defined trace element partition coefficients for titanite, apatite and monazite, showing that, for example, those for apatite and titanite can be sensitive to changes in SiO_2 and the Aluminium Saturation Index of the initial magma (Prowatke and Klemme, 2005, 2006b). Based on granitoid samples, apatite and titanite trace element chemistry has also been shown to closely reflect the composition of the host magma (Chu et al., 2009; Jennings et al., 2011; Bruand et al., 2016) and yields information about petrogenetic processes that is not always apparent at the whole rock scale (mixing, in-situ crystal fractionation, metasomatism; e.g. Belousova et al., 2002; Mcleod et al., 2011; Zirner et al., 2015). Such phases can occasionally be dated by U-Pb chronology (e.g. Storey et al., 2007; Chew and Donelick, 2012) and the Zr-in-titanite thermometer (Hayden et al., 2008) is robust where a buffered equilibrium mineral assemblage is present. Therefore, trace element concentrations and isotope systems in accessory minerals other than zircon (e.g. apatite, titanite, monazite) can provide useful insights to magma petrogenesis and crustal growth.

Lately, development of SIMS instruments and the availability of characterized standards provide an opportunity to analyse in-situ O isotope ratios in apatite and titanite (King et al., 2001; Trotter et al., 2008; Bonamici et al., 2014; Sun et al., 2016). Unlike for zircon, such O isotope datasets are currently extremely limited (Bindeman, 2008, e.g. King et al., 2001 for igneous and metamorphic rocks and Bonamici et al., 2011, 2014, 2015 for titanite in metamorphic rocks). Based on three sets of samples, King et al. (2001) report a zircon-titanite oxygen isotope fractionation factor of $\sim 1.2 \pm 0.3‰$ at 650 °C for magmatic rocks. They report a second equilibrium fractionation factor of $\sim 2.1 \pm 0.4‰$ calculated on a limited number of metamorphic rocks ($n = 5$) of unknown temperature (maximum greenschist facies conditions). Bonamici et al. (2011, 2014) recently interpreted oxygen isotope profiles through titanite to infer the cooling history of metamorphic rocks. So far as apatite is concerned, although oxygen isotope analysis in bioapatite is a well-developed palaeoenvironmental technique (e.g. Trotter et al., 2008), data concerning magmatic and metamorphic apatite are almost non-existent (Farver and Giletti, 1989).

Experimental studies (e.g. Farver and Giletti 1989; Zhang et al., 2006) have evaluated oxygen diffusion mechanisms within accessory minerals. Farver (2010) reviewed experimental data highlighting that diffusion rates in accessory minerals are slower than in common igneous rock-forming minerals. Zhang et al. (2006) have shown that oxygen diffusion in titanite is isotropic but that two diffusion mechanisms can occur, depending on the morphology of the titanite crystals. Experiments with synthetic euhedral crystals reveal only self diffusion in the titanite lattice. On the other hand, oxygen diffusion in crystals lacking euhedral morphology could be driven by two mechanisms: self diffusion in the lattice and diffusion along a fast plane such as a planar defect. Zhang et al. (2006) have also shown that closure temperature of titanite to oxygen diffusion is about 600 °C for a titanite crystal with a radius <200 μm, using wet diffusion data with a typical upper crust cooling rate of 10 °C/Ma. For apatite, experiments have highlighted a strong anisotropy of oxygen diffusion (e.g. Farver and Giletti, 1989; Brenan, 1994). Farver and Giletti (1989) estimated that the diffusion coefficient for transport parallel to the c axis is about three orders of magnitude greater than for diffusion perpendicular to the c axis under similar conditions. They also implied that water could play a significant role. Finally, diffusion of halogens and oxygen in apatite has also been shown to be faster than diffusion of other key elements (e.g. Sr, Mn, Pb, REE; Cherniak, 2010). In summary, although oxygen diffusion in accessory minerals is generally slower than in the main rock-forming minerals, diffusion in apatite is faster than titanite which is faster than zircon (for similar grain sizes, cooling rates and in hydrous conditions). Therefore, it is expected that metamorphic processes (>550 °C, Farver and Giletti, 1989) could promote faster oxygen diffusion in apatite than in the other accessory phases. Notwithstanding these previous experimental studies, there is clearly still a lot to learn about oxygen isotope behaviour in natural systems.

For this contribution we have analysed O isotopes, major and trace elements in coexisting zircon, titanite and apatite from different sets of granitoids of different ages (Caledonian high Ba-Sr granites, Archean sanukitoids and Cadomian BADR). The reason for their selection is as follows. There is a major point of current discussion concerning when and how the Earth evolved from the Archean TTG production to modern arc magma. Our sample sets form part of an ongoing investigation into evolving subduction processes across geological time, from late Archean sanukitoids to modern arc-related magmas. High Ba-Sr granitoids are the Phanerozoic equivalent of sanukitoids. Both require the presence of a metasomatised mantle wedge and sanukitoids therefore imply the onset of steep subduction at 2.9–2.7 Ga (e.g. Martin et al, 2005). The Cadomian BADR suite represents typical arc-related magmatism prevalent throughout the Proterozoic and Phanerozoic. Using such rocks, we can also evaluate the isotopic information that accessory minerals record on petrogenesis and post-magmatic processes. For this purpose, we first compare oxygen isotope behaviour in apatite and titanite on a well-constrained cogenetic high Ba-Sr suite (mafic-felsic) of fresh, unmetamorphosed samples affected by crystal fractionation as indicated by trace element variations. This set of samples allows investigation of magmatic equilibration between zircon, apatite and titanite, definition of $\delta^{18}O$ fractionation factors between the phases and constraint of the effects of crystal fractionation on $\delta^{18}O$. Subsequent to this, we compare with the variably deformed and metamorphosed Proterozoic and Archean equivalents to test the minerals' robustness to resetting. Our results

suggest that titanite and apatite oxygen isotope ratios can record useful information from various stages in the history of their host granitoids, from petrogenesis and source signature to later overprinting processes such as metamorphism and fluid circulation.

2. SAMPLE DESCRIPTION

2.1. High Ba-Sr granitoids and appinites (Scotland)

The high Ba-Sr granitoids and appinites studied for this contribution were selected from a suite of late Caledonian plutons from the Northern Highlands of Scotland (Strontian and Rogart localities; Fowler et al., 2008). These plutonic rocks were derived from variably enriched subcontinental lithospheric mantle and their compositions range from appinitic through granodiorite to granite. Six granitoids (SR1, SR3, SR4, RT1, R2, RHG1) and two appinites (RA1 and SR2) have been studied for this work. Their whole rock chemistry, O, Sr and Nd isotopic characteristics were described by Fowler et al. (2001, 2008) and detailed petrography and chemistry of the accessory minerals by Bruand et al. (2014). These plutons have high Ba-Sr contents, are rich in light rare earth elements (LREE), have low Nb, Ta and heavy rare earth element (HREE) abundances. Thus, they share the main characteristics of sanukitoids (Archean granitoids; Martin et al., 2005). Petrological characteristics can be found in Table 1 and in Bruand et al. (2014). The main accessory phases are zircon, apatite and titanite. Zircon in granitoids has typical igneous oscillatory zoning. The only difference between Strontian and Rogart zircons is the presence of an occasional darker rim in the Rogart locality. In the mafic samples (SR2, RA1), there are only rare zircon grains with oscillatory or sector zoning. In granitoids, apatite is oscillatorily zoned (Fig. 1c-f) while apatite in the appinite usually has a dark core partly resorbed and a brighter thin rim (Fig. 1g, h, j; Table 1). Titanite in granitoids is usually large (>500 μm in diameter) and euhedral. Strontian titanite occasionally has a thin darker rim (Fig. 2e and f). Titanite in the appinites is anhedral and has sector zoning (Fig. 2j).

2.2. Sanukitoids from the Karelia province (Finland)

Sanukitoids belong to a group of plutonic rocks that appeared in the Late Archaean to Archean-Proterozoic transition and have been linked to major geodynamic changes at that time (Laurent et al., 2014). Geochemists and petrologists agree that they result from the interaction between a mantle wedge and a metasomatic agent (either oceanic crust melt or sediments). In this work, samples from two well characterised sanukitoid localities from the Karelia Province (Finland) have been studied (San 316 and and A572, respectively Koitere and Arola localities in Heilimo et al., 2011). They have been dated at 2.7 Ga (U-Pb on zircon; Heilimo et al., 2011) and whole rock geochemical data, oxygen and hafnium isotopes in zircon are available (Heilimo et al., 2010, 2013). They have been interpreted as the result of the interaction between the depleted mantle wedge and a recycled crustal component during slabbreakoff at the end of subduction (Heilimo et al., 2013). Sample A572 is from the Arola locality and is a K-feldspar porphyritic granodiorite. Sample San 316 is from the Koitere locality and is a large feldspar porphyroclast-bearing graniodorite with preserved ortho- and clinopyroxene. Samples from both localities have been affected by amphibolite to granulite facies metamorphism. Sample A572 has also been affected by later multiple overprinting metamorphism and alteration events (Hölttä and Heilimo, 2017). Details of the petrography can be found in Table 1. The main accessory minerals in these samples are zircon, apatite, titanite ± epidote and opaques. Zircon in these samples has typical igneous oscillatory zoning with a darker rim. Zircon can locally be heavily altered. Apatite generally has faint oscillatory zoning (Fig. 1l). Some A572 apatite crystals contain sharper zoning with a bright core and a darker rim (Fig. 1k). Titanite in A572 sample is euhedral and has oscillatory zoning. Its core is darker and seems more altered with locally abundant cracks within the crystals. Titanite in San 316 is anhedral and has a broad homogeneous core and a thin dark rim (Fig. 2m). Occasional sector and oscillatory zoning occurs.

2.3. Guernsey igneous complex (Channel Islands)

Guernsey is part of the Armorican Massif and is divided geologically into two main parts. The southern part mainly comprises Paleoproterozoic gneisses (the Icartian gneisses; Samson et al., 2003) intruded by syntectonic and subsequently deformed Neoproterozoic granitoids (Perelle quartz-diorite and l'Erée granite; Samson and D'Lemos, 1999), and the northern part is dominated by the undeformed, Neoproterozoic Northern Igneous Complex. Samples studied here are from deformed and undeformed granitoids, allowing the effects of deformation and fluid circulation to be constrained.

2.3.1. Undeformed sample from the Northern Igneous Complex

Plutonic rocks from the Northern Igneous Complex have a calc-alkaline signature and were emplaced at the end of the Cadomian orogeny (c.a. 560–550 Ma; De Bremond d'Ars et al., 1992). They are referred to by Brown et al. (1990) as post-tectonic units. One sample from the Northern Igneous Complex has been selected for this study, taken from the Bordeaux diorite (BD-02). It comprises hornblende, quartz and feldspar with minor chlorite and white mica (Table 1). Accessory phases are epidote, zircon, apatite and titanite. In cathodoluminescence (CL) images, apatite has a heavily disturbed core with a thin darker rim (Fig. 1a). Zircon is small (<150 μm in length) with dark oscillatory zoning. Locally, zircon crystals can be significantly altered. In backscattered-electron imaging (BEI) titanite is anhedral with a bright core and a darker thin rim (usually < 50 μm).

2.3.2. Deformed sample from the l'Erée granite

A sample from l'Erée granite (EG-07) in the southern part of the island was also studied. This locality was previously described by Topley et al. (1990) as "ambiguous

Table 1
Sample description for the studied granitoids/appinites in the High Ba-Sr localities, sanukitoids from the Karelia Province (Finland) and the igneous complex from Guernsey (Channel Islands). GPS coordinates are given in the WGS84 format. Mineral abbreviations are from (Whitney and Evans, 2010).

	Sample	Locality	Rock type	Age (Ma)	Major rock forming minerals	Accessory minerals	References	GPS coordinates
High Ba-Sr (Scotland)	R2	Rogart	Tonalite	425	hb-fsp-qz-bt-mu	zircon, apatite, titanite (euhedral), allanite	Bruand et al. (2014), Fowler et al. (2001, 2008)	Lat 57.996508 N Long 4.185728 W
	RA1	Rogart	Appinite		hb-cpx-fsp-bt ± cal	zircon, apatite, titanite (Anhedral)		Lat 58.029738 N Long 4.133559 W
	RT1	Rogart	Tonalite		hb-fsp-qz-bt-mu ± aln	zircon, apatite, titanite (euhedral), allanite		Lat 57.993611 N Long 4.197395 W
	RGH1	Rogart	Granite		fsp-bt-qz ± chl-cal	zircon, apatite, titanite (euhedral)		Lat 58.010645 N Long 4.250916 W
	SR1	Strontian	Granodiorite	425	hb-fsp-bt-qz	zircon, apatite, titanite (euhedral)		Lat 56.689443 N Long 5.602272 W
	SR2	Strontian	Appinite		hb-fsp-bt ± cal	zircon, apatite, titanite (anhedral)		Lat 56.689443 N Long 5.602272 W
	SR3	Strontian	Granodiorite		hb-fsp-bt-qz	zircon, apatite, titanite (euhedral), allanite		Lat 56.685100 N Long 5.627994 W
	SR4	Strontian	Granodiorite		hb-fsp-qz-bt ± chl	zircon, apatite, titanite (euhedral), allanite		Lat 56.730766 N Long 5.540805 W
Sanukitoids (Karelian Province)	A572	Arola	Granodiorite	2723	fsp-bt-qz	zircon, apatite, titanite (euhedral), epidote	Heilimo et al (2013)	Lat 64.44985108 N Long 29.00994815E
	San316	Koitere	Granodiorite	2722	hb-fsp-qz-bt-px-opx	zircon, apatite, titanite (anhedral), opaques	Heilimo et al. (2011)	Lat 63.22764732 N Long 30.65472253E
Igneous Complex (Guernsey)	EG07	l'érée granite	Granite	614	fsp-qz-hb-chl	zircon, apatite, titanite (euhedral)	unpub.data in Samson et al. (2003)	Lat 49.454750 N Long 2.655250 W
	BD02	Port Infer	Diorite	560–550	hb-qz-fsp ± chl-micas	zircon, apatite, titanite (anhedral), epidote		Lat 49.490000 N Long 2.578361 W

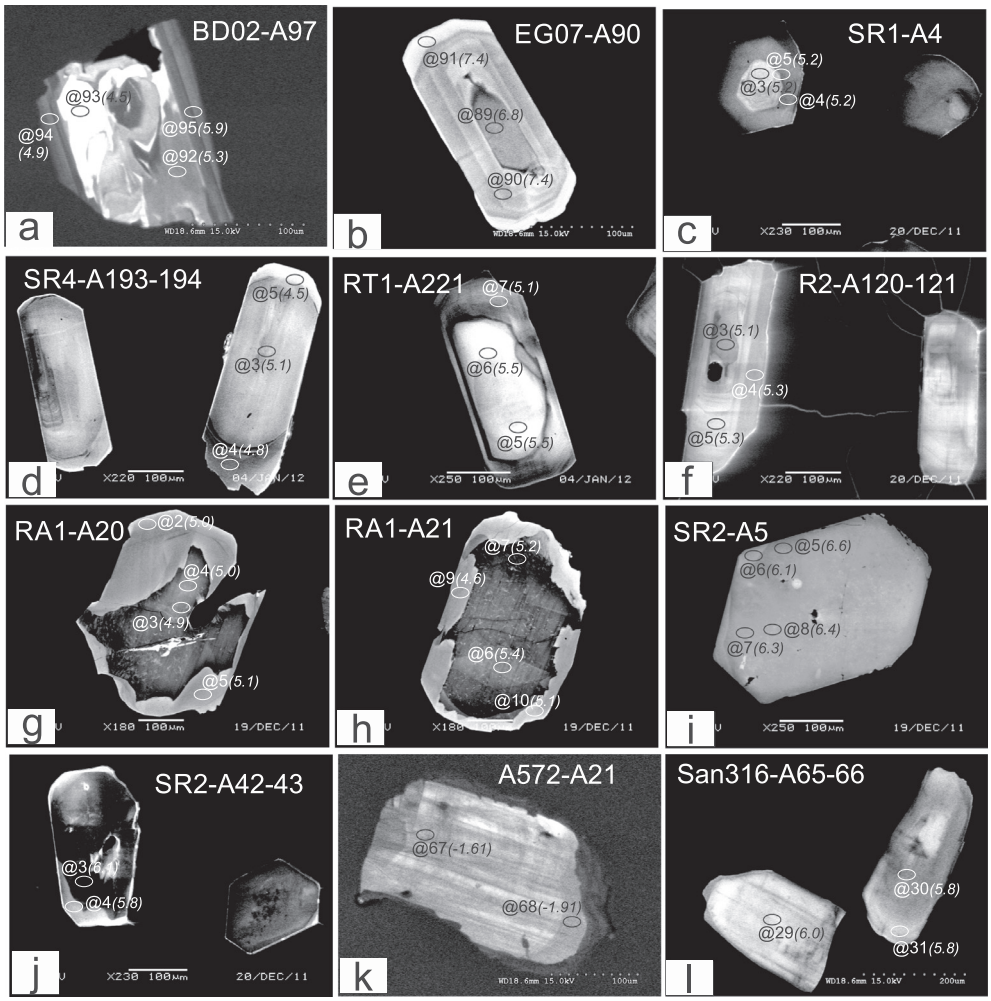

Fig. 1. Representative cathodoluminescence pictures of apatite crystals for Guernsey samples (A, B), High Ba-Sr samples (C–J) and sanukitoids (K, L). Reported ionprobe analyses (results in italic and ‰) can be found Table 2.

regarding the distinction between the Southern and the Northern complexes". However, field relationships (e.g. the presence of dykes absent in the north and the presence of foliation) indicate that it belongs to the early Cadomian event and intruded the Icartian basement syntectonically. This is also suggested by a zircon U-Pb crystallisation age of 614 Ma ± 2 Ma (Samson et al., 2003). The early Cadomian intrusions in the Channel Islands are also calc-alkaline in composition and have typical volcanic arc granite signatures (Power et al., 1990). This sample is mainly made up of feldspar, quartz, hornblende and chlorite (Table 1). Accessory minerals are zircon, apatite and titanite. Apatite and zircon have well-defined oscillatory zoning. In CL images, apatite usually has a dark core and a brighter rim (Fig. 1b). Zircon has typical igneous oscillatory zoning with locally with a darker thin rim (<10 μm). Titanite is euhedral and large (up to 500 μm in diameter). Its core is rich in inclusions and BEI reveals local dark patchy zonation, interpreted as alteration (Fig. 2c). Well-defined oscillatory zoning is present in the outermost part of the crystal (Fig. 2c).

3. ANALYTICAL TECHNIQUES

3.1. Image acquisition

Mineral separates of apatite, titanite and zircon from the studied samples were picked and mounted in epoxy resin. The grains were distributed no further from 0.5 cm from the centre of the mount which was polished as flat as possible to avoid analytical bias during oxygen isotope analysis (e.g. Kita et al., 2009). The mounts exposed the centre of the grains in order to observe as much of the internal zonation as possible. Apatite grains were mounted with orientations parallel to and perpendicular to the c axis to test potential bias of oxygen isotope data with different crystallographic orientations. During our analytical sessions, we analysed in both directions (parallel and perpendicular to c axis) but could not find a systematic relationship. Zircon and apatite were imaged using cathodoluminescence (CL) with a KeDev Centaurus CL detector housed on a JEOL 6060LV scanning electron microscope (SEM) or a Philips XL 30 SEM at the University of Portsmouth (accelerating

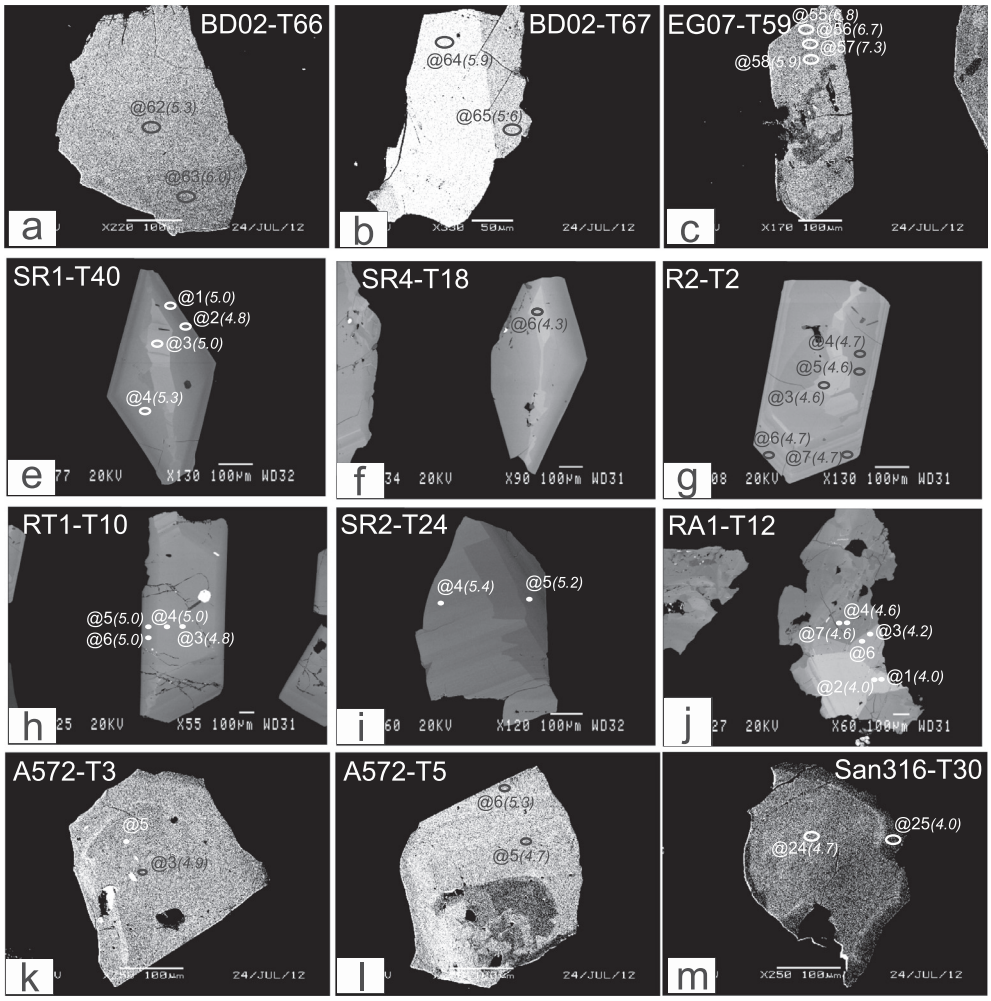

Fig. 2. Representative back-scattered pictures of titanite crystals for Guernsey samples (A–C), High Ba-Sr samples (E–J) and sanukitoids (K–M). Reported ionprobe analyses (results in italic and ‰) can be found Table 2.

voltage15 kV). Back-scattered electron (BSE) images for titanite were performed using a JEOL JSM-6100 or a Philips XL 30 SEM also at the University of Portsmouth at 20 kV.

3.2. Secondary Ion Mass Spectrometer analysis (SIMS)

SIMS analysis of oxygen isotope ratios was performed at the Edinburgh Ion Microprobe Facility (EIMF) using a Cameca 1270 mass spectrometer operating with a primary Cs^+ beam, which was focussed to a spot with a diameter of ca.10 μm, operating at conditions of 10 kV and ~6nA for the Cs beam. Data presented in this study were acquired over 9 analytical sessions (Sessions 1–5 over 5 continous days and sessions 6–9 over 4 continuous days, see Appendix A.2. for details). Instrumental calibration for each session was done by analyzing Kahn and/or Tibor standards for titanite, Durango for apatite and 91500 for zircon. Details of standards can be found in the supplementary data (Appendix A.1). Instrumental mass fractionation and instrument drift were monitored by repeat analyses of Kahn/Tibor for titanite, Durango for apatite and 91500 and Temora 2 for zircon. Raw $\delta^{18}O$ of standards for each session were normalised to the accepted values (10.07‰ for 91500; 8.50‰ for Durango, 10.52‰ for Kahn and −0.30‰ for Tibor) and for drift. The same corrections were applied to the samples - details of the different sessions, standard values and drift corrections can be found in Appendix A.2. Repeatabilities of the standards for each sessions are also reported in A.2. and for each sample in Table 2 (for Durango: 0.3‰ 2SD for sessions 2–3, 0.6‰ 2SD for session 7, 0.4‰ 2SD for session 9; for ttn standards: 0.2‰ 2SD for session 1, 0.3‰ 2SD for session 2 and 0.4‰ 2SD for session 8; for 91500 0.2‰ 2SD for sessions 4–5 and 0.3‰ 2SD for session 6). Bonamici et al. (2011, 2014) have shown that instrumental mass fractionaton (IMF) can be dependent on Ti in the octahedral site for titanite. Khan (Ti a.p.f.u. = 0.83) and Tibor (Ti a.p.f.u = 0.97) runs were analysed at the beginning of each session to monitor the dependence on Ti of IMF. The titanite compositions studied in this work vary over the same Ti a.p.f.u. range (0.88–0.94). For the three titanite sessions, compositional variations showed no correlations with IMF (Appendix A.1). Trotter et al. (2008) have suggested that

Table 2
Compilation of oxygen data aquire for the different studied samples. δ ^{18}Ocorr values are δ ^{18}O corrected from the drift. Details of the different sessions and standards are available in Appendix A.2.

Sple	FileName	d18O corr.	error (SD) on spot (2σ)	Sple	FileName	d18O corr.	error (SD) on spot (2σ)	Sple	FileName	d18O corr.	error (SD) on spot (2σ)
	TITANITE				BMttn@3*	4.16	0.32		ttn@18	4.64	0.53
	HIGH BA-SR				BMttn@4*	4.61	0.35	**A572**	**Average**	**4.92**	**n = 14**
SR1	SMttn@1*	5.05	0.24		BMttn@6*	4.30	0.32		**2SD**	**0.62**	
	SMttn@2*	4.84	0.28		BMttn@7*	4.58	0.32	**San316**	ttn@21	4.06	0.53
	SMttn@3*	4.99	0.28	**RA1**	**Average**	**4.27**	**n = 6**		ttn@22	4.45	0.52
	SMttn@4*	5.26	0.28		**2SD**	**0.55**			ttn@23	5.06	0.52
	SMttn@5	4.91	0.26	**RGH1**	SMttn@1	5.51	0.23		ttn@24*	4.68	0.53
	BMttn@1	4.97	0.33		SMttn@2	5.17	0.24		ttn@25*	4.01	0.53
	BMttn@2	4.82	0.33		SMttn@3	5.16	0.24		ttn@26	5.18	0.53
	BMttn@3	5.14	0.33		SMttn@4	5.17	0.28		ttn@27	4.54	0.53
	BMttn@4	4.26	0.32	**RHG1**	**Average**	**5.25**	**n = 4**		ttn@28	5.36	0.52
	BMttn@5	4.35	0.32		**2SD**	**0.35**			ttn@29	4.60	0.54
	BMttn@6	4.07	0.31	**R2**	BMttn@3*	4.57	0.31		ttn@30	4.11	0.52
SR1	**Average**	**4.79**	**n = 12**		BMttn@4*	4.74	0.33	**San316**	**Average**	**4.61**	**n = 10**
	2SD	**0.77**			BMttn@5*	4.59	0.33		**2SD**	**0.95**	
SR2	SMttn@2	5.56	0.24		BMttn@6*	4.72	0.32				
	SMttn@3	5.31	0.26		BMttn@7*	4.72	0.33		**GUERNSEY**		
	SMttn@4*	5.42	0.25	**R2**	**Average**	**4.67**	**n = 5**	**EG07**	ttn@46	7.61	0.54
	SMttn@5*	5.17	0.23		**2SD**	**0.16**			ttn@48	6.69	0.53
SR2	**Average**	**5.36**	**n = 4**	**RT1**	BMttn@1	4.51	0.32		ttn@49	7.32	0.55
	2SD	**0.33**			BMttn@2	4.67	0.31		ttn@50	7.05	0.53
SR3	SMttn@1	5.37	0.28		BMttn@3*	4.77	0.33		ttn@51	7.53	0.53
	SMttn@2	5.38	0.28		BMttn@4*	5.03	0.33		ttn@52	7.03	0.53
	SMttn@3	5.28	0.26		BMttn@5*	5.01	0.33		ttn@53	7.20	0.54
	SMttn@4	5.30	0.24		BMttn@6*	4.96	0.34		ttn@55*	6.85	0.53
	SMttn@5	5.07	0.25	**RT1**	**Average**	**4.83**	**n = 6**		ttn@56*	6.74	0.52
SR3	**Average**	**5.28**	**n = 5**		**2SD**	**0.42**			ttn@57*	7.29	0.55
	2SD	**0.25**							ttn6@58*	6.86	0.53
SR4	BMttn@1	4.48	0.39		**SANUKITOIDS**			**EG07**	**Average**	**7.11**	**n = 11**
	BMttn@2	4.39	0.38	**A572**	ttn@1	5.02	0.53		**2SD**	**0.62**	
	BMttn@3	4.08	0.43		ttn@3*	4.88	0.52	**BD02**	ttn@60	5.77	0.54
	BMttn@4*	4.28	0.41		ttn@5*	4.75	0.54		ttn@61	5.90	0.55
	BMttn@5*	4.36	0.40		ttn@6*	5.29	0.55		ttn@62*	5.34	0.53
	BMttn@6	4.32	0.42		ttn@7	4.72	0.56		ttn@63*	6.02	0.54
	BMttn@8*	4.33	0.30		ttn@8	4.59	0.54		ttn@64*	5.87	0.54
	BMttn@9	4.25	0.35		ttn@10	5.23	0.54		ttn@65*	5.59	0.54

	BMttn@10	4.32	0.33
	BMttn@11*	3.89	0.35
SR4	**Average**	**4.27**	**n = 10**
	2SD	**0.34**	
RA1	BMttn@1*	4.01	0.32
	BMttn@2*	3.98	0.33
	APATITE		
	HIGH BA-SR		
SR1	APM@3*	5.24	0.46
	APM@4*	5.21	0.41
	APM@5*	5.16	0.40
	APM@6	5.37	0.39
	APM@7	5.63	0.39
SR1	**Average**	**5.32**	**n = 5**
	2SD	**0.38**	
SR2	BMAP@3	5.72	0.42
	BMAP@5*	6.56	0.40
	BMAP@6*	6.11	0.37
	BMAP@7*	6.34	0.42
	BMAP@8*	6.43	0.42
	BMAP@9	5.73	0.43
	BMAP@10	6.00	0.39
	APM@3*	6.15	0.41
	APM@4*	5.80	0.39
	APM@7	5.78	0.43
	APM@8	6.03	0.46
	APM@9	6.26	0.41
	APM@10	5.86	0.45
SR2	**Average**	**6.06**	**n = 13**
	2SD	**0.55**	
SR3	APM@1	5.94	0.44
	APM@2	5.76	0.41
	APM@4	6.11	0.42
	APM@5	5.79	0.43
	APM@6	5.87	0.43
	APM@7	5.41	0.45
SR3	**Average**	**5.81**	**n = 6**
	2SD	**0.47**	
SR4	APM@3*	5.09	0.41
	APM@4*	4.81	0.41
	ttn@11	5.19	0.56
	ttn@12	4.90	0.53
	ttn@13	4.70	0.53
	ttn@14	5.05	0.54
	ttn@16	5.51	0.54
	ttn@17	4.42	0.53
	APM@2	4.96	0.45
	APM@3	5.38	0.38
	APM@4	5.22	0.39
	APM@5	4.97	0.43
	APM@6	5.27	0.41
RA1	**Average**	**5.09**	**n = 14**
	2SD	**0.40**	
RHG1	APM@1	6.06	0.41
	APM@2	6.07	0.44
	APM@3	5.76	0.41
	APM@4	5.64	0.41
	APM@5	5.63	0.43
RHG1	**Average**	**5.83**	**n = 5**
	2SD	**0.44**	
R2	APM@2	5.39	0.44
	APM@3*	5.06	0.40
	APM@4*	5.28	0.44
	APM@5*	5.30	0.43
R2	**Average**	**5.26**	**n = 4**
	2SD	**0.28**	
RT1	APM@1	5.58	0.43
	APM@2	5.17	0.41
	APM@3	5.49	0.38
	APM@4	5.22	0.41
	APM@5*	5.49	0.38
	APM@6*	5.49	0.42
	APM@7*	5.11	0.43
	APMRT1@8	5.17	0.37
	APMRT1@9	5.19	0.43
RT1	**Average**	**5.32**	**n = 9**
	2SD	**0.37**	
	SANUKITOIDS		
	San316		
	AP@26	5.85	0.70
	ttn@66	5.90	0.54
	ttn@67	5.50	0.55
BD02	**Average**	**5.74**	**n = 8**
	2SD	**0.47**	
	AP@43	1.73	0.73
	AP@44	−0.10	0.74
	AP@45	0.13	0.75
	AP@46	−0.76	0.73
	AP@47	0.16	0.78
	AP@48	0.40	0.75
	AP@67*	−1.61	0.62
	AP@68*	−1.91	0.60
	AP@69	−0.69	0.60
	AP@70	−1.87	0.64
	AP@71	−1.09	0.61
	AP@72	−1.48	0.62
	AP@73	−1.72	0.59
	AP@74	−0.98	0.62
	AP@75	−1.17	0.61
	AP@76	−1.55	0.63
A572	**Average**	**−0.79**	**n = 17**
	2SD	**1.95**	
	GUERNSEY		
	EG-07		
	AP@54	7.00	0.68
	AP@55	6.56	0.71
	AP@56	6.93	0.74
	AP@57	7.58	0.68
	AP@58	7.66	0.71
	AP@59	6.22	0.68
	AP@60	6.33	0.71
	AP@61	6.07	0.76
	AP@62	7.53	0.72
	AP@63	6.08	0.69
	AP@64	7.32	0.67
	AP@65	7.12	0.74
	AP@66	6.98	0.73
	AP@77	6.12	0.61

(*continued on next page*)

Table 2 (*continued*)

Sple	FileName	d18O corr.	error (SD) on spot (2σ)
	APM@5*	4.52	0.42
	APM@6	4.18	0.42
	APM@7	4.54	0.41
SR4	**Average**	**4.63**	**n = 5**
	2SD	**0.68**	
RA1	BMAP@2*	5.02	0.45
	BMAP@3*	4.93	0.43
	BMAP@4*	5.01	0.42
	BMAP@5*	5.10	0.42
	BMAP@6*	5.38	0.43
	BMAP@7*	5.23	0.41
	BMAP@9*	4.64	0.43
	BMAP@10*	5.09	0.41
	APM@1	5.08	0.41
	AP@94*	4.88	0.62
	AP@95*	5.90	0.62
BD02	**Average**	**5.13**	**n = 4**
	2SD	**1.21**	
	ZIRCON		
	HIGH BA-SR		
SR1	ZRM@1	5.86	0.32
	ZRM@2	5.77	0.30
	ZRM@4	5.98	0.29
	ZRM@5	6.04	0.28
	ZRM@3	6.13	0.29
	ZRM@4	6.05	0.30
	ZRM@5	6.22	0.29
SR1	**Average**	**6.01**	**n = 7**
	2SD	**0.31**	
SR2	ZRM@1	5.82	0.31
	ZRM@3	5.95	0.31
	ZRM@4	5.89	0.30
	ZRM@5	5.55	0.31
	ZRM@6	5.93	0.29
	ZRM@7	5.61	0.28
	ZRM@8	5.94	0.31
	AP@27	5.42	0.70
	AP@28	5.42	0.71
	AP@29*	6.05	0.74
	AP@30*	5.79	0.73
	AP@31*	5.79	0.69
	AP@32	5.64	0.70
	AP@33	6.55	0.70
	AP@34	5.41	0.69
	AP@35	6.07	0.67
	AP@101	5.76	0.60
San316	**Average**	**5.80**	**n = 11**
	2SD	**0.69**	
	A572		
	AP@42	−0.94	0.70
	ZRM@7	6.27	0.30
SR4	**Average**	**6.28**	**n = 7**
	2SD	**0.20**	
RA1	ZRM@1	5.66	0.30
	ZRM@2	5.47	0.33
RA1	**Average**	**5.57**	**n = 2**
	2SD	**0.26**	
RHG1	ZRM@1	6.20	0.30
	ZRM@2	5.99	0.29
	ZRM@3	5.76	0.30
	ZRM@6	6.00	0.30
	ZRM@7	5.91	0.31
	ZRM@8	6.40	0.29
	ZRM@9	6.03	0.32
	ZRM@10	5.98	0.34
	ZRM@3	6.19	0.37
	ZRM@4	6.01	0.30
	ZRM@5	5.98	0.32
RHG1	**Average**	**6.04**	**n = 11**
	2SD	**0.34**	
R2	ZRM-@1	6.32	0.32
	ZRM-@2	5.56	0.30
	AP@78	7.22	0.62
	AP@79	6.71	0.62
	AP@80	6.37	0.63
	AP@81	6.33	0.60
	AP@83	7.42	0.63
	AP@86	6.05	0.56
	AP@89*	6.76	0.57
	AP@90*	7.45	0.64
	AP@91*	7.38	0.63
EG07	**Average**	**6.83**	**n = 23**
	2SD	**1.11**	
	BD02		
	AP@92*	5.26	0.60
	AP@93*	4.47	0.60
	ZR@4	6.40	0.43
	ZR@5	6.01	0.41
	ZR@10	5.82	0.41
	ZR@11	6.28	0.41
	ZR@12	6.14	0.46
	ZR@13	6.36	0.43
	ZR@14	6.33	0.42
	ZR@15	6.51	0.43
	ZR@6	5.51	0.42
	ZR@7	5.81	0.41
A572	**Average**	**6.10**	**n = 12**
	2SD	**0.59**	
San316	ZR-@39	7.59	0.39
	ZR-@40	7.35	0.41
	ZR-@41	7.67	0.43
	ZR-@43	6.95	0.39
	ZR-@44	7.70	0.38
San316	**Average**	**7.45**	**n = 5**
	2SD	**0.63**	
	GUERNSEY		
EG07	ZR@45	8.09	0.39
	ZR-@46	7.89	0.39

	ZRM@9	5.60	0.30		ZRM-@3	6.58	0.30		ZR@47	8.27	0.39
	ZRM@1	6.15	0.30		ZRM-@4	6.17	0.30		ZR@48	8.42	0.43
	ZRM@2	5.90	0.30		ZRM-@5	6.17	0.31		ZR@50	8.63	0.43
	ZRM@3b	6.01	0.29		ZRM-@6	5.95	0.32		ZR@51	7.70	0.55
	ZRM@4b	5.92	0.31		ZRM-@7	5.66	0.34		ZR@52	7.84	0.40
	ZRM@5	5.69	0.30		ZRM@1	5.74	0.31		ZR@54	8.10	0.40
	ZRM@9	6.03	0.32		ZRM@4	5.63	0.32		ZR@55	7.56	0.44
	ZRM@10	6.12	0.32		ZRM@7	5.73	0.31		ZR@56	8.35	0.43
SR2	**Average**	**5.87**	**n = 15**	**R2**	**Average**	**5.95**	**n = 10**		ZR@57	7.93	0.39
	2SD	**0.37**			**2SD**	**0.69**			ZR@58	8.27	0.43
SR3	ZRM@1	5.67	0.29	**RT1**	ZRM@1	5.93	0.31	**EG07**	**Average**	**8.09**	**n = 12**
	ZRM@2	5.58	0.31		ZRM@2	6.09	0.28		**2SD**	**0.63**	
	ZRM@3	5.88	0.30		ZRM@3	6.20	0.29	**BD02**	ZR@71	5.65	0.45
	ZRM@4	5.90	0.29		ZRM@6	6.01	0.32		ZR@72	5.57	0.52
	ZRM@5	5.40	0.33		ZRM@7	5.99	0.29		ZR@73	5.36	0.45
	ZRM@6	5.70	0.30		ZRM@3	6.33	0.30		ZR@74	5.53	0.48
SR3	**Average**	**5.69**	**n = 6**		ZRM@4	6.57	0.30		ZR@76	5.52	0.43
	2SD	**0.38**			ZRM@5	6.33	0.31		ZR@77	5.66	0.45
SR4	ZRM@1	6.37	0.29		ZRM@6	6.53	0.32	**BD02**	**Average**	**5.55**	**n = 6**
	ZRM@2	6.36	0.28	**RT1**	**Average**	**6.22**	**n = 9**		**2SD**	**0.22**	
	ZRM@3	6.14	0.27		**2SD**	**0.47**					
	ZRM@4	6.26	0.28		**SANUKITOIDS**						
	ZRM@5	6.16	0.32	**A572**	ZR@1	5.98	0.42				
	ZRM@6	6.38	0.31		ZR@2	6.01	0.42				

* Analysis Visible on Figs. 1 and 2.

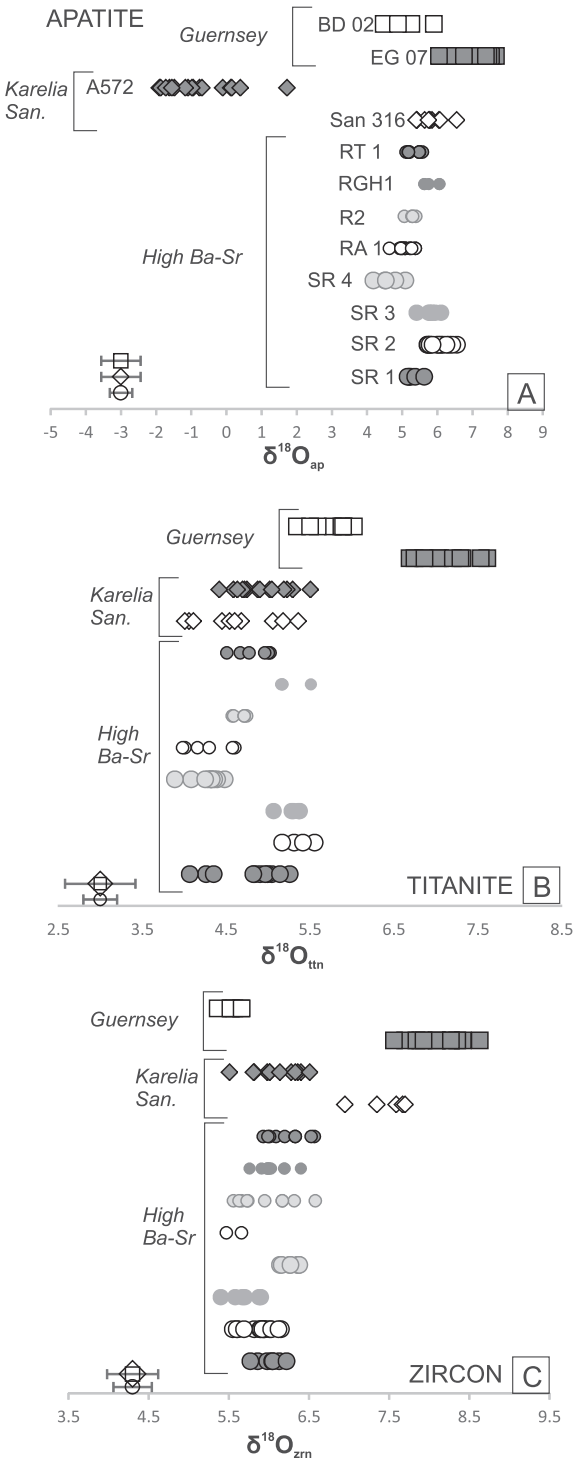

Fig. 3. δ ^{18}O results sorted by minerals (Table 2). A – for apatite, B – titanite and C – zircon. Empty symbols with error bars are repeatability of the standards (Durango for Apatite, Khan and/or Tibor for titanite and 91,500 for zircon) for the different sessions.

instrumental mass fractionaton (IMF) between Durango fluorapatite, other fluorapatites measured, and shark teeth was absent in SHRIMP analyses. However, later Sun et al. (2016) suggested that a variation of 1% of CaO in Durango apatite could lead to up to 3‰ heavier δ^{18}O. It has to be noted that they could only see this effect in one of their standard grains and that based on their dataset, a correlation could not be further quantitatively defined. During our analytical sessions, Durango was analysed with a repeatability between 0.3 and 0.6 2SD while CaO varied between 53.4 and 55% (See Appendix A.3). The matrix effect suggested by Sun et al. (2016) was therefore not observed during our analytical sessions. Durango is a fluorapatite such as all the apatite crystals analysed during this work. Considering 2% uncertainty on the microprobe analyses, our unknowns have a similar CaO range to Durango (A.3.) although P_2O_5 is much more variable in our samples (Durango: P_2O_5 = 39.7–41.7 wt%; unknowns range = 39.3–47.4 wt%). Finally, monitoring CaO and P_2O_5 vs δ^{18}O for the High Ba-Sr suite did not highlight a matrix effect (Appendix A.3). Other potential matrix effects have been investigated using titanite and apatite compositional data but except for one appinite sample (RA1, see Section 5.1.4) no systematic variation between chemistry of the phases and oxygen isotope values has been observed (Appendix A.3).

3.3. Major and trace elements analysis

Major and trace elements in both apatite and titanite were analysed in the same part of the crystal based on zoning (identified by BSE or CL), and within 10–20 μm of the oxygen analysis spot. Detailed analytical techniques (electron microprobe analysis and laser ablation-inductively coupled plasma mass spectrometry) can be found in Bruand et al. (2014). Major and trace element analyses for apatite and titanite corresponding to oxygen isotopes spots in this study are available in Appendix A.3.

4. RESULTS

Oxygen isotopes have been measured in the range of accessory minerals (apatite, zircon, titanite) present in the studied samples (Table 2). Each of the studied crystals was imaged by BSE or by CL (Figs. 1 and 2) and the different zones observed have been analysed when spatial resolution allowed. In this section, we present oxygen isotope data of the three phases by locality.

4.1. δ ^{18}O in the high Ba-Sr suite

In the high Ba-Sr cogenetic suite, δ $^{18}O_{zrn}$ in the granitoids (RT1, R2, RHG-1, SR1, SR3, SR4) have comparable average values between 5.7‰ and 6.2‰ and are within uncertainty of each other. Most samples have 2SD close to the uncertainties of the standards except for RT1(6.2‰ ± 0.5 2SD) and R2 (6.0‰± 0.7 2SD). In the case of sample R2, the scatter seems related to the zoning of the zircon crystals. Notably, the darker rims tend to have the lowest values (Appendix A.4). No systematic relationship between the larger scatter of sample RT1 and the texture/composition of the zircon could be identified. The mafic samples have homogeneous δ $^{18}O_{zrn}$ values within uncertainty of

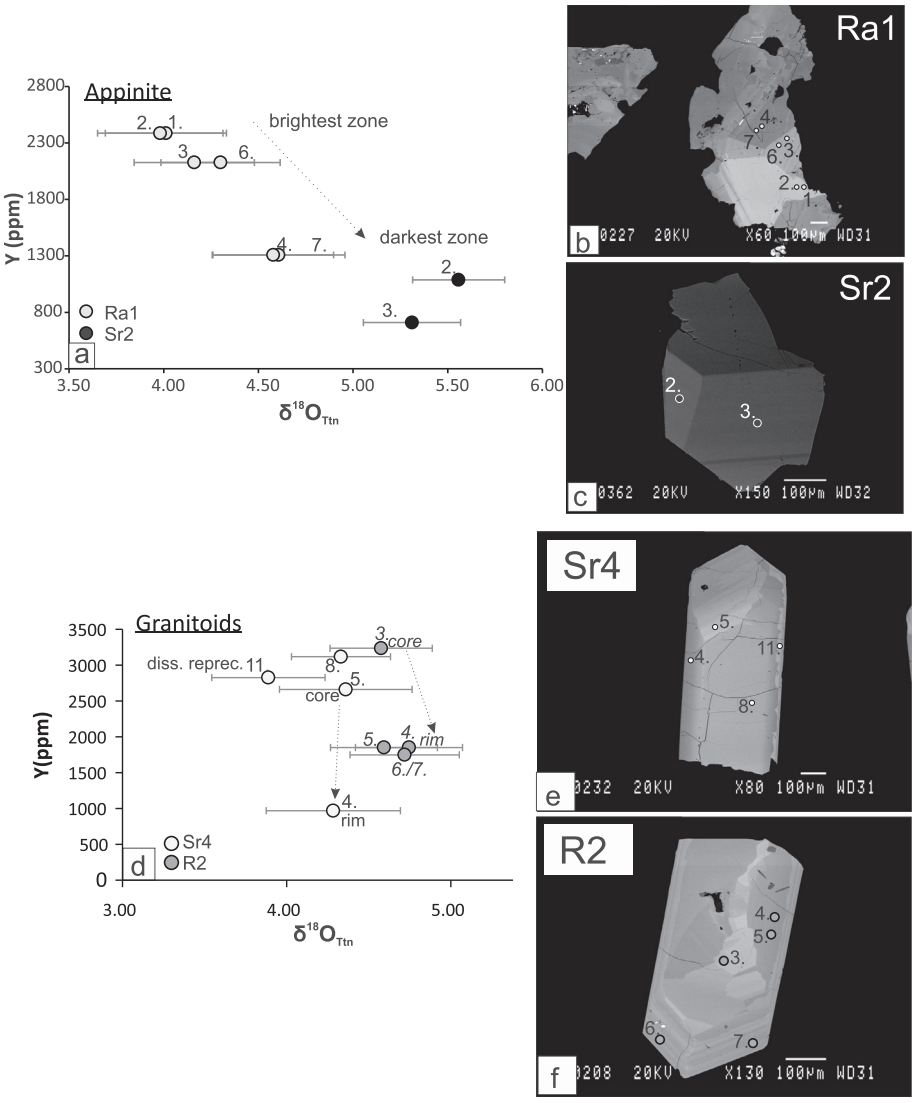

Fig. 4. A – Y vs δ $^{18}O_{ttn}$ for *appinnites* for 2 crystals from the High Ba-Sr samples, for B – RA1 and C – SR2 crystals in sector zoning. The figure reveals decreasing δ $^{18}O_{ttn}$ values from the brighest to the darkest zones of the sector zoning. D – Y vs δ $^{18}O_{ttn}$ for granitoids for 2 crystals from the High Ba-Sr samples, for E – SR4 and F – R2 crystals from core to rim. The figure reveals comparable δ $^{18}O_{ttn}$ values from core to rim with a typical oscillatory zoning. Reported trace element and δ $^{18}O_{ttn}$ data are in Appendix A.3.

the granitoids (5.9‰ ± 0.4 2SD for SR2 and 5.6‰ ± 0.3 2SD for RA1, Table 2).

δ $^{18}O_{ap}$ for samples R2, RA1, RT1 and SR1 average ca. 5.‰ with uncertainties within standard repeatability (<0.4‰, Fig. 3a, Table 2). RGH1, SR2 and SR3 have slightly higher values averaging ca. 5.9‰, and a slightly higher scatter $0.4 < 2SD < 0.6$. Considering uncertainties, these samples have comparable δ $^{18}O_{ap}$ values. Sample SR4 has a lower average value (4.6‰) with significant variability (±0.7 2SD). For this sample, cores and rims of apatite were analysed and there is no systematic correlation with the wider variability observed in the oxygen isotope data.

δ $^{18}O_{ttn}$ average values obtained on the high Ba-Sr suite for most samples form a tight cluster between 4.7‰ and 5.4‰. RA1 and SR4 have slightly lower average values (4.3‰ for both samples). Two samples (SR1 and RA1) have significantly larger uncertainties than the standard repeatability (>0.4‰ 2SD). In detail, the scatter of SR1 data is mainly attributed to 3 analyses on the same crystal (BMttn@4 to 6, Fig. 3b, Appendix A.2). The scatter for sample RA1 highlights a different process. RA1 titanite crystals are anhedral (Table 1) with sector zoning, which correlates with strong elemental variation such as Y (Fig. 4 a-c), CaO and TiO_2 (Appendix A.3). The highest Y values correspond to the lowest oxygen isotope values and *vice versa* (although δ $^{18}O_{ttn}$ are within 2SD uncertainties; Fig. 4 c). Similar observations could not be made on anhedral SR2 titanite crystals as the oxygen isotope data and the trace element dataset on this sample are limited (Table 2, Appendix A.3).

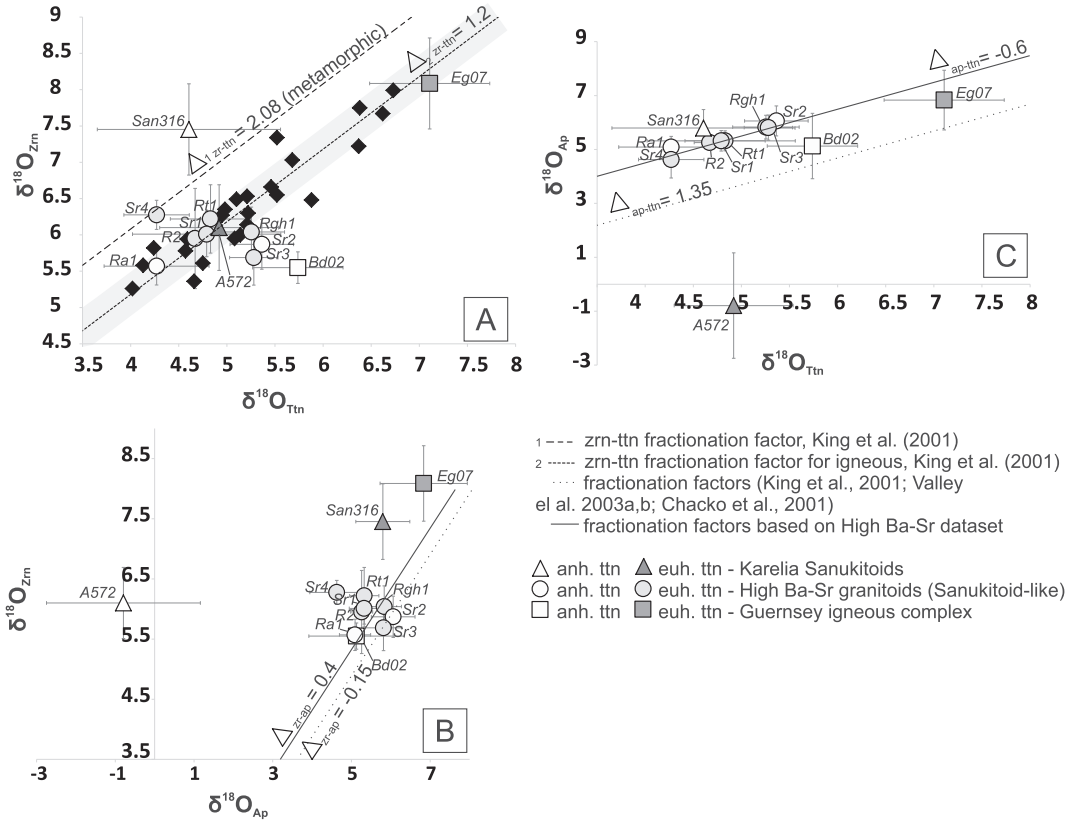

Fig. 5. Compilation of apatite, titanite and zircon. δ ^{18}O for the different samples studied in this contribution (Table 2). A – δ $^{18}O_{zrn}$ vs δ $^{18}O_{ttn}$, factor fractionation for igneous (1.2 ± 0.3, grey field) and metamorphic rocks from the literature have been reported (King et al., 2001), B – δ $^{18}O_{zrn}$ vs δ $^{18}O_{ap}$, C- δ $^{18}O_{ap}$ vs δ $^{18}O_{ttn}$. Fractionation factors for the High Ba-Sr dataset are calculated based on the average of all High Ba-Sr samples (Appendix A.3.).

4.2. δ ^{18}O in sanukitoids

In the Karelia province samples, δ $^{18}O_{zrn}$ data obtained on A572 range between 5.5 and 6.5‰, whereas San 316 has higher values between 7 and 7.7‰ (Fig. 3c). These values are within the range of previous data from Karelia province sanukitoid zircons (5.1‰ ± 0.6‰ 2SD to 7.1‰ ± 0.4‰ 2 SD; Heilimo et al., 2013).

San316 has δ $^{18}O_{ap}$ of 5.8 ± 0.7 2SD with repeatability close to that of the standard (0.6 2SD on Durango). A572 has a heavily disturbed signature with values close to or below zero, and a significant scatter (±2.0 2SD; Table 2). No chemical or obvious petrographic observations could be found to explain these negative values.

Average δ $^{18}O_{ttn}$ obtained on the sanukitoid samples are similar and range between 4.6‰ (±1.0 2SD) for San 316 and 4.9‰ (±0.6 2SD) for A572. They both have larger uncertainties than the standard (0.4 2SD). Titanite crystals in San 316 are anhedral and have oscillatory zoning. In this sample, core to rim systematics can locally be observed with the rims up to 0.7‰ lower than the cores (@24 core, @25 rim in Table 2, Appendix A.3).

4.3. δ ^{18}O in Guernsey arc magmas

In the *deformed* granite sample EG-07 from Guernsey, δ ^{18}O of the three accessory phases have the highest values of our entire dataset but also reveal a wide range of values for each accessory mineral compared to the *undeformed* sample. δ $^{18}O_{zrn}$ is variable (8.1‰ ± 0.6 2SD) when compared to the reapeatibility of the standard (0.3 2SD, Table 2). Similarly, δ ^{18}O in apatite has variable values ranging from 6.1‰ to 7.7‰ (Fig. 3A, Table 2). The average δ $^{18}O_{ttn}$ is 7.1‰ ± 0.6 2SD but closer to the standard uncertainties (0.4 2SD; Fig. 3B; Table 2). Backscattered electron imaging of titanite reveals heavily altered cores and a high density of cracks, which could potentially explain the scatter of titanite δ ^{18}O (Fig. 2c), but these are absent in zircon and apatite (e.g. Fig. 1b).

The *undeformed* Guernsey samples BD-02 has lower and less disturbed δ ^{18}O values for zircon and titanite with uncertainties on the different grains close to the uncertainties of the standards (Appendix A.2, Table 2). δ $^{18}O_{zrn}$ is 5.6‰ ± 0.2 2SD and δ $^{18}O_{ttn}$ has an average of 5.7‰ ± 0.5 2SD. δ $^{18}O_{ap}$ on the other hand varies significantly and ranges from 4.5‰ to 5.9‰. CL imaging of these apatite grains reveals patchy zoning characteristic of fluid-mediated alteration (Fig. 1a).

5. DISCUSSION

In order to establish whether δ ^{18}O of titanite and/or apatite can be used reliably to derive δ ^{18}O of the parent magma, it is important to test whether and how δ $^{18}O_{mineral}$

can be influenced by factors such as crystal face development and diffusion, crystal fractionation, temperature or metamorphism/alteration. Initially, the unmetamorphosed samples (high Ba-Sr suite) are discussed in the light of isotopic equilibrium between zircon and the other accessory minerals, crystal face development and crystal fractionation. Following this, the metamorphosed sanukitoids (Karelia province) and the arc magma samples (Guernsey) are used to discuss the impact of metamorphism, deformation and fluid alteration on accessory mineral $\delta^{18}O$.

5.1. The unmetamorphosed high Ba-Sr suite

5.1.1. Zircon-titanite fractionation factor

Understanding if the measured phases are at magmatic equilibrium is fundamental to the understanding of the behaviour of $\delta\ ^{18}O_{mineral}$ in the different sets of samples studied here. In this section, equilibrium is tested by comparing measured $\delta\ ^{18}O$ of the different accessory phases to existing fractionation factors proposed for these phases. Following this, observed magmatic disequilibrium is discussed, considering processes such as crystal shape, metamorphism and fluid circulation, which could promote diffusion.

Shown in Fig. 5a are published $\delta\ ^{18}O$ zircon and titanite data and zircon-titanite fractionation factors from King et al. (2001) (1.2 ± 0.3‰ for igneous systems for a temperature of 650 °C; 2.1 ± 0.4‰ for metamorphic systems) and the data from this study. King et al. (2001) use the equation:

$$\Delta_{zrn-ttn} = 1.02 * 10^6/T^2(T\ in\ K)$$

which for a range of temperatures between 650 °C and 850 °C gives fractionation factors between 1.2 and 0.8, respectively (Appendix A.3). The high Ba-Sr suite data plot in close accordance with the former of these. However, the uncertainties on the data are of the same order as the fractionation factor difference for a 650–850 °C temperature range. This means that any temperature effect within the 650–850 °C range is negligible compared to the uncertainty in the data. In contrast to this close correspondence, previous experimental work on $\Delta_{zrn-ttn}$ such as that by Zheng (1993) has used different equations that give fractionation factors ranging between −0.15 and −0.10 respectively, for the same temperature range. This suggests that such experimental work may not be directly applicable to natural systems.

5.1.2. Zircon-apatite fractionation factor.

There are no published empirical calibrations of oxygen isotope fractionation between igneous apatite and zircon. However, Valley et al. (2003) defined 'A factors' for the apatite-zircon pair, derived from a combination of King et al. (2001) and Valley (2003) empirical values plus experimental work from calcite and mineral exchange from Chacko et al. (2001). Using such A_{zrn-ap} gives $\Delta_{zr-ap} = -0.15$ at 650 °C (Appendix A.3).

In Fig. 5b, $\delta\ ^{18}O_{zrn}$ against $\delta\ ^{18}O_{ap}$ are plotted to monitor potential disequilibrium. Most high Ba-Sr samples are within or close to the 2SD repeatability of the standard (<0.5 2SD) and measured phases are consistent with each other. Except sample SR4, the high Ba-Sr suite defines a tight cluster. Based on these samples, calculated fractionation factors range between −0.2 and 1.65 (average $\Delta_{zrn-ap} = 0.4 \pm 0.6$‰ 1SD) within which range sits the recalculated $\Delta_{zrn-ap} = -0.15$ by Valley et al (2003). The systematically lower value of SR4 is difficult to explain; one possibility could be that apatite is not in equilibrium with zircon. This explanation is unlikely as in this type of evolved magma, apatite and zircon are usually early co-crystallising phases (Hoskin et al., 2000). This has been confirmed by Bruand et al. (2014) using trace elements in accessory phases for similar samples from this locality (SR1 and SR3). Sample SR4 is not altered and does not show any evidence of significant interaction with fluid. The only mineralogical difference from the other high Ba-Sr granitoids is the presence of pyrrhotite inclusions within the cores of the apatite crystals, implying locally reducing conditions of the magma (e.g. Tepper and Kuehner 1999). Speculatively, these redox conditions may be responsible for changes in the OH bonding within apatite.

5.1.3. Fractionation factor of apatite-titanite

Compiling all the data for the well equilibrated titanite and apatite of the high Ba-Sr suite reveals a strong correlation between the two phases, with an average fractionation factor Δ_{ap-ttn} of 0.6 (±0.1‰ 1SD; Fig. 5c and Appendix A.3). This result is very different to what can be derived from Valley (2003 and references therein): $\Delta_{ap-ttn} = 1.35$ at 650 °C and $\Delta_{ap-ttn} = 0.91$ at 850 °C (Appendix A.3). Given the very limited available data, the origin of this inconstitency in fractionation factors is unclear.

5.1.4. The influence of compositional and sector zoning on $\delta\ ^{18}O$ titanite

Titanite crystals can be strongly zoned (oscillatory, sector, fir-tree), and previous studies have shown that although the most enriched sector zones are out of equilibrium (e.g. fir-tree zoning; Watson and Liang, 1995; Hayden et al., 2008), other parts with oscillatory zoning are not and can be used to monitor magmatic processes such as in-situ fractionation, contamination or mixing, or magmatic parameters such as temperature of crystallisation (Hayden et al., 2008; Mcleod et al., 2011; Bruand et al., 2014). During the oxygen isotope analytical sessions, we tested the influence of highly contrasting zones observable in BSE images, by systematically analysing for major and trace elements plus oxygen isotopes.

Bruand et al. (2014) showed that titanite crystals from high Ba-Sr granitoids record progressive decrease of REE, Nb and Ta toward the rim of the crystal. In order to investigate the compositional zoning influence on $\delta^{18}O$, Y is used as a proxy for REE (with the knowledge of a strong correlation – Bruand et al., 2014). At both high Ba-Sr localities, REE and Y concentrations in granitoid titanite decrease from core to rim while $\delta^{18}O_{titanite}$ is constant (Fig. 4d). Bruand et al. (2014) also showed that occasional darker rims only found in SR1 and SR3 samples (e.g. Fig. 2e) recorded a late event of mixing with local mafic magma. $\delta^{18}O_{titanite}$ from these darker rims did not differ from the

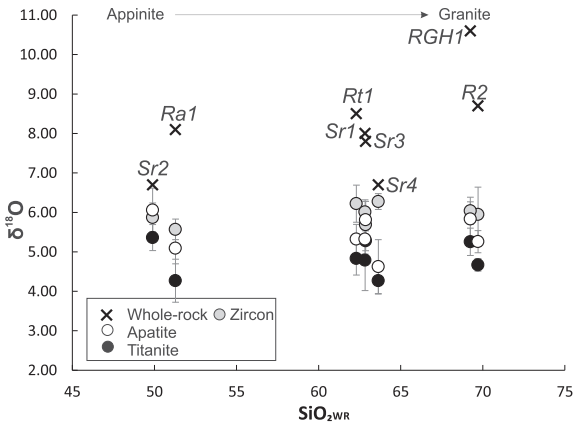

Fig. 6. δ ^{18}O vs SiO_{2WR} for high Ba-Sr samples showing the crystal fractionation influence on whole rock, apatite, titanite and zircon. δ ^{18}O values are the average values presented in Table 2 and SiO_{2WR} values are from Fowler et al. (2008) and personal XRF data.

core of the crystal (Fig. 2e; δ $^{18}O_{ttn}$ = 5‰ from core toward the dark rim).

In the appinites (SR2 and RA1, Fig. 4), titanite is anhedral and a late phase with interstitial texture and well-developed sector zoning. In one large sector zoned crystal of RA1, δ $^{18}O_{ttn}$ data is anti-correlated with Y content, the brightest parts of the sector zoning having lowest δ $^{18}O_{ttn}$ values (Fig. 4, albeit with variations close to reproducibility constraints). Such anti-correlation between δ $^{18}O_{ttn}$ and Y content was not observed in other anhedral titanite grains across our range of samples (BD02 in Guernsey, San 316 in the sanukitoids), but in these cases, titanite crystals show evidence for either disequilibrium or resetting. Since previous work on sector zoning in titanite has also shown that the brightest parts of the sector zoning are out of equilibrium for trace elements (e.g. Hayden et al., 2008), in future work, caution should be taken when analysing the brightest parts of sector zoning as the most enriched parts of the sector zones could suggest disequilibrium.

5.1.5. Does crystal fractionation influence accessory mineral δ ^{18}O?

Since it has been argued that the Caledonian high Ba-Sr granite suite is the result of progressive crystal fractionation from the appinitic compositions toward the most differentiated granites (Fowler et al., 2001, 2008), and apatite-titanite are at equilibrium, our data can be used to examine the influence of crystal fractionation on δ $^{18}O_{apatite}$ and δ $^{18}O_{titanite}$. The studied samples have closely similar Sr and Nd radiogenic isotopic values (see Fowler et al., 2001, 2008), and thus the influence of open-system behaviour (such as assimilation of the local metasediments) is thought to be minor. Available δ ^{18}O whole rock data (Fowler et al., 2001, 2008) are mostly within a 6.7–8.7‰ range from the most mafic endmenber (appinite) to felsic compositions (Fig. 6). RHG1 has a higher δ ^{18}O whole rock value (10.6‰) which is interpreted to be the result of late feldspar alteration (Fowler et al., 2001; Bruand et al., 2014).

In Fig. 6, SiO_{2WR} is used to monitor the potential effect of crystal fractionation on oxygen isotopes in apatite and titanite. Across the range of compositions from ca. 50 to ca. 70% SiO_2, δ $^{18}O_{zircon}$ ranges between 5.9‰ and 6.3‰ and are all within uncertainty (Table 2). Similarly, Fig. 6 reveals that there are no variations of oxygen isotopic values resolvable between the less and the most differentiated samples for apatite and titanite. Therefore, extensive crystal fractionation seems not to influence accessory mineral δ ^{18}O.

5.2. Archean sanukitoids from Karelia

Zircon crystals from Karelia (A572 and San316) are magmatic and retain original δ ^{18}O (Heilimo et al., 2013). Therefore, the fractionation factors defined above can be used to determine whether δ ^{18}O of titanite and apatite have been disturbed during their prolonged metamorphic history.

5.2.1. The influence of metamorphism/fluid circulation on δ ^{18}O titanite

Titanite crystals in San316 (and the other sanukitoid, A572) show igneous oscillatory zoning, occasionally surrounded by a thin and dark (metamorphic) rim (<10 μm, Fig. 2m). Titanite ages of 2707 Ma from A572 are comparable with solution-based zircon ages, confirming their igneous history (Hyppönen 1983), but similar affirmation is not possible for San316 for which titanite ages are lacking. Trace element data on titanite cores for both samples are similar and consistent with igneous compositions (Sr/Sm < 0.2, Appendix A.3; Bruand et al., 2014). δ ^{18}O in sample San316 overlaps a metamorphic zircon-titanite fractionation factor of 2.1 (Fig. 5a) previously defined by King et al. (2001), and is clearly out of magmatic equilibrium with respect to δ $^{18}O_{zrn}$. This metamorphic empirical fractionation factor was defined using 5 samples and is poorly constrained to date.

It therefore seems clear that, although the San316 titanite trace element signature is igneous, oxygen isotopes have been partly reset during the metamorphism which affected this Archean terrane. The small size (<200 μm) and anhedral shape could have promoted diffusional resetting of oxygen isotopes and explain the significant scatter of titanite data for this sample (Fig. 3b). This is consistent with previous experimental studies on oxygen diffusion in titanite which have shown that oxygen diffusion in non euhedral crystals could be faster as it is impacted by two mechanisms, self diffusion in the lattice, and diffusion along a fast plane (Zhang et al., 2006). For example, Zhang et al. (2006) calculated that at about 500 °C, a titanite core with a grain radius similar to our grain size (200 μm) will retain the original $^{18}O/^{16}O$ for only about 2.7 Ma.

On the other hand, sample A572 which has been affected by similar metamorphism has δ $^{18}O_{ttn}$ average values consistent with magmatic equilibrium (Fig. 5a). The uncertainties on the data are slightly outside the 2SD of the standard, which suggests that oxygen diffusion during metamorphism could have played a minor role. In any case, titanite crystals in this sample are euhedral and large (>200 μm, up to

500 μm), and seem to better resist diffusion than San316 crystals.

5.2.2. The influence of fluid circulation/metamorphism on δ ^{18}O apatite

In Fig. 5b and c, sample A572 plots remote from the main correlation, indicating disequilibrium between apatite and zircon or titanite. Its anomalous negative δ $^{18}O_{ap}$ values can only be explained by interactions with meteoric or hydrothermal waters - the only reservoirs with significantly negative δ ^{18}O (0 to −55; Eiler 2001; Valley et al., 2005). The lack of preserved pyroxene in the mineralogy and the presence of altered feldspar supports an interpretation of late hydrothermal interaction (Table 1).

On the other hand, in Fig. 5b, San316 has an average δ $^{18}O_{ap}$ of 5.80 ± 0.7 2SD, with uncertainties close to the standard repeatability for this session (2SD of 0.6). This is consistent with the highest zircon-apatite fractionation factor defined from the high Ba-Sr samples (0.9–1.2‰). Thus, in this sample apatite is in equilibrium with zircon and, contrary to titanite from the same sample, metamorphism seems not to have reset δ $^{18}O_{ap.}$

To summarise, results demonstrate that both titanite and apatite can be affected by resetting due to metamorphism/fluid circulation, but that they may behave independently. The difference could potentially be related to different type of fluid. For example, previous workers (e.g. Ayers and Watson 1991) have shown that apatite is not easily dissolved by high P-T fluid unless this fluid is acidic. Therefore one could potentially explain the complete resetting of apatite of sample A572 by the dissolution and reprecipitation of apatite by an acidic fluid.

5.3. Deformed vs undeformed arc magmas from Guernsey

In Fig. 5a-b, average values of δ $^{18}O_{ap}$ and δ $^{18}O_{ttn}$ of sample EG07 plot within the general set of data previously defined by the high Ba-Sr dataset and are therefore in magmatic equilibrium with respect to δ $^{18}O_{zrn}$. However, the uncertainties on the average δ $^{18}O_{ap}$ and δ $^{18}O_{ttn}$ values are beyond analytical uncertainty. EG-07 is deformed, rich in chlorite and has heavily altered feldspar. Titanite cores are altered and show dark patchy zoning. These observations suggest fluid circulation promoted by deformation, which has disturbed the δ ^{18}O signature in both accessory phases.

In contrast, the undeformed sample (BD02) has δ $^{18}O_{ttn}$ that is clearly in disequilibrium with respect to δ $^{18}O_{zrn}$ (Fig. 5a). It has not experienced significant metamorphism but contains small, anhedral titanite crystals. Therefore, the disequilibrium between titanite and zircon in this sample is more likely due to the small size of the grains. Following Zhang et al. (2006) anhedral shape could also promote faster diffusion processes.

On the other hand, sample BD02 has average δ $^{18}O_{ap}$ values consistent with magmatic $\Delta_{zrn\text{-}ap}$ defined by the high Ba-Sr samples. However, they also show significant scatter beyond analytical uncertainty (Fig. 3a and Fig. 5b). Textural observations indicate that apatite in this sample has patchy cores and these have the lowest δ $^{18}O_{ap}$ values (4.5‰; Fig. 1a). Thin dark rims have the highest δ $^{18}O_{ap}$ (5.9‰). Patchy zoning is unusual for igneous rocks but described in fluid related conditions (e.g. Zhang et al., 2017). We therefore interprete the values obtained in the core as related to fluid circulation during the magmatic stage.

In summary, the study of the unmetamorphosed Guernsey samples reveal that fluid circulation during either the magmatic stage or during later deformation can promote partial resetting of δ $^{18}O_{ap}$ and δ $^{18}O_{ttn}$.

6. CONCLUSIONS

The analysis of zircon, apatite and titanite within three sets of samples from different geological settings, formed at different times highlights the following important findings:

- δ ^{18}O of titanite is in equilibrium with zircon across our three sets of samples except when titanite is anhedral and small in size (<200 μm). Thus titanite is a robust mineral preserving the original magmatic δ ^{18}O.
- δ ^{18}O of apatite records magmatic δ ^{18}O in the high Ba-Sr samples, but is more prone to partial or complete resetting when affected by metamorphism, deformation and/or fluid circulation.

The presented dataset demonstrates that apatite and titanite can potentially record original magmatic δ ^{18}O of a sample in different geological contexts. However, in-depth study of the zoning features and petrology of the samples is important to constrain the history of the sample. Our results open new opportunities to investigate the magmatic but also the resetting history of granitoids through time by analysing δ ^{18}O of apatite and titanite. Indeed, several authors have recently reported the importance of apatite inclusions protected within zircon to better constrain magmatic conditions of the early Earth (Bruand et al., 2016; Delavault et al., 2016; Emo et al., 2018).

ACKNOWLEDGEMENTS

We are grateful to Stuart Kearns for the help provided with the microprobe analyses, to Geoff Long for amazing technical support. We are extremely grateful to John Craven for the help provided with the ion probe analyses. This is a contribution to International Geoscience Programme (IGCP) 599. This work was supported by the Natural Environment Research Council (grant NE/I025573/1) and by the French Government Laboratory of Excellence initiative n° ANR-10-LABX-0006, the Region Auvergne and the European Regional Development Fund. This is Laboratory of Excellence ClerVolc contribution number 335. We deeply thank the editor A. Nemchin and three anonymous reviewers for their input.

APPENDIX A. SUPPLEMENTARY MATERIAL

Supplementary data to this article can be found online at https://doi.org/10.1016/j.gca.2019.04.002.

REFERENCES

Ayers J. C. and Watson E. B. (1991) Solubility of apatite, monazite, zircon, and rutile in supercritical aqueous fluids with implications for subduction zone geochemistry. *Philos. Trans. Phys. Sci. Eng.* **335**, 365–375.

Bell E. A., Harrison T. M., Mcculloch M. T. and Young E. D. (2011) Early Archean crustal evolution of the Jack Hills Zircon source terrane inferred from Lu – Hf, 207 Pb/206 Pb, and d 18 O systematics of Jack Hills zircons. *Geochim. Cosmochim. Acta.* **75**, 4816–4829. https://doi.org/10.1016/j.gca.2011.06.007.

Belousova E. A., Griffin W. L., O'Reilly S. Y. and Fisher N. I. (2002) Apatite as an indicator mineral for mineral exploration: trace-element compositions and their relationship to host rock type. *J. Geochem. Explor.* **76**, 45–69. https://doi.org/10.1016/S0375-6742(02)00204-2.

Belousova E. A., Griffin W. L. and O'Reilly S. Y. (2006) Zircon crystal morphology, trace element signatures and Hf isotope composition as a tool for oetrogenetic modelling: examples from Eastern Australian granitoids. *J. Petrol.* **47**, 329–353. https://doi.org/10.1093/petrology/egi077.

Belousova E. A., Kostitsyn Y. A. and Griffin W. L., et al. (2010) The growth of the continental crust: constraints from zircon Hf-isotope data. *Lithos* **119**, 457–466. https://doi.org/10.1016/j.lithos.2010.07.024.

Bindeman I. (2008) Oxygen isotopes in mantle and crustal magmas as revealed by single crystal analysis. *Rev. Mineral Geochem.* **69**, 445–478. https://doi.org/10.2138/rmg.2008.69.12.

Bonamici C. E., Kozdon R., Ushikubo T. and Valley J. W. (2011) High-resolution P-T-t paths from δ18O zoning in titanite: a snapshot of late-orogenic collapse in the Grenville of New York. *Geology* **39**, 959–962. https://doi.org/10.1130/G32130.1.

Bonamici C. E., Kozdon R., Ushikubo T. and Valley J. W. (2014) Intragrain oxygen isotope zoning in titanite by SIMS: cooling rates and fluid infiltration along the Carthage-Colton Mylonite Zone, Adirondack Mountains, NY, USA. *J. Metamorph. Geol.* **32**, 71–92. https://doi.org/10.1111/jmg.12059.

Bonamici C. E., Fanning C. M. and Kozdon R., et al. (2015) Combined oxygen-isotope and U-Pb zoning studies of titanite: new criteria for age preservation. *Chem. Geol.* **398**, 70–84. https://doi.org/10.1016/j.chemgeo.2015.02.002.

Brenan J. (1994) Kinetics of fluorine, chlorine and hydroxyl exchange in fluorapatite. *Chem. Geol* **110**, 195–210.

Brown M., Power G. M., Topley C. G. and D'Lemos R. S. (1990) Cadomian magmatism in the North Armorican Massif. *Geol. Soc. Lond. Spec. Publ.* **51**, 181–213. https://doi.org/10.1144/GSL.SP.1990.051.01.12.

Bruand E., Storey C. and Fowler M. (2014) Accessory mineral chemistry of high Ba-Sr granites from Northern Scotland: constraints on petrogenesis and records of whole-rock Signature. *J. Petrol.*. https://doi.org/10.1093/petrology/egu037.

Bruand E., Storey C. and Fowler M. (2016) An apatite for progress: Inclusions in zircon and titanite constrain petrogenesis and provenance. *Geology*. https://doi.org/10.1130/G37301.1.

Chacko T., Cole D. R. and Horita J. (2001) Equilibrium oxygen, hydrogen and carbon isotope fractionation factors applicable to geologic systems. *Rev. Mineral Geochem.* **43**, 1–81.

Cherniak D. J. (2010). *Diffusion in Accessory Minerals* **vol. 72**, 827–869. https://doi.org/10.2138/rmg.2010.72.18.

Chew D. M. and Donelick R. a. (2012) Combined apatite fission track and U-Pb dating by LA-ICP-MS and its application in apatite provenance analysis. *Mineral Assoc. Canada Short Course* **42**, 219–247.

Chu M. F., Wang K. L. and Griffin W. L., et al. (2009) Apatite composition: tracing petrogenetic processes in Transhimalayan granitoids. *J. Petrol.* **50**, 1829–1855. https://doi.org/10.1093/petrology/egp054.

de Bremond d'Ars , Martin H., Auvray B. and Lécuyer C. (1992) Petrology of a magma chamber: the Plutonic Complex of Guernsey (Channel Islands, UK). *J. Geol. Soc. London* **149**, 701–708. https://doi.org/10.1144/gsjgs.150.4.0788.

Delavault H., Dhuime B. and Hawkesworth C. J., et al. (2016) Tectonic settings of continental crust formation: insights from Pb isotopes in feldspar inclusions in zircon. *Geology* **44**, 1–4. https://doi.org/10.1130/G38117.1.

Dhuime B., Hawkesworth C. J., Cawood P. A. and Storey C. D. (2012) A change in the geodynamics of continental growth 3 billion years ago. *Science* **335**(6074), 1334–1336. https://doi.org/10.1126/science:1216066.

Eiler J. M. (2001) Oxygen isotope variations of basaltic lavas and upper mantle rocks. *Rev. Mineral Geochem.* **43**, 319–364. https://doi.org/10.2138/gsrmg.43.1.319.

Emo R. B., Smit M. A. and Schmitt M., et al. (2018) Science Direct Evidence for evolved Hadean crust from Sr isotopes in apatite within Eoarchean zircon from the Acasta Gneiss Complex. *Geochim. Cosmochim. Acta* **235**, 450–462. https://doi.org/10.1016/j.gca.2018.05.028.

Farver J. R. and Giletti B. J. (1989) Oxygen and strontium diffusion kinetics in apatite and potential applications to thermal history determinations. *Geochim. Cosmochim. Acta* **53**, 1621–1631. https://doi.org/10.1016/0016-7037(89)90243-3.

Farver J. R. (2010). In *Oxygen and Hydrogen Diffusion in Minerals*, pp. 447–507. https://doi.org/10.2138/rmg.2010.72.10.

Fowler M. B., Henney P. J., Darbyshire D. P. F. and Greenwood P. B. (2001) Petrogenesis of high Ba-Sr granites: the Rogart pluton, Sutherland. *J. Geol. Soc. London* **158**, 521–534. https://doi.org/10.1144/jgs.158.3.521.

Fowler M. B., Kocks H., Darbyshire D. P. F. and Greenwood P. B. (2008) Petrogenesis of high Ba-Sr plutons from the Northern Highlands Terrane of the British Caledonian Province. *Lithos* **105**, 129–148. https://doi.org/10.1016/j.lithos.2008.03.003.

Gregory C. J., McFarlane C. R. M., Hermann J. and Rubatto D. (2009) Tracing the evolution of calc-alkaline magmas: In-situ Sm-Nd isotope studies of accessory minerals in the Bergell Igneous Complex, Italy. *Chem. Geol.* **260**, 73–86. https://doi.org/10.1016/j.chemgeo.2008.12.003.

Grimes C. B., Wooden J. L., Cheadle M. J. and John B. E. (2015) " Fingerprinting " tectono – magmatic provenance using trace elements in igneous zircon. *Contrib. Mineral Petrol.* **170**, 1–26. https://doi.org/10.1007/s00410-015-1199-3.

Hayden L. A., Watson E. B. and Wark D. A. (2008) A thermobarometer for sphene (titanite). *Contrib. Mineral Petrol.* **155**, 529–540. https://doi.org/10.1007/s00410-007-0256-y.

Heilimo E., Halla J. and Hölttä P. (2010) Discrimination and origin of the sanukitoid series: geochemical constraints from the Neoarchean western Karelian Province (Finland). *Lithos* **115**, 27–39. https://doi.org/10.1016/j.lithos.2009.11.001.

Heilimo E., Halla J. and Huhma H. (2011) Single-grain zircon U-Pb age constraints of the western and eastern sanukitoid zones in the Finnish part of the Karelian Province. *Lithos* **121**, 87–99. https://doi.org/10.1016/j.lithos.2010.10.006.

Heilimo E., Halla J., Andersen T. and Huhma H. (2013) Neoarchean crustal recycling and mantle metasomatism: Hf-Nd-Pb-O isotope evidence from sanukitoids of the Fennoscandian shield. *Precambr. Res.* **228**, 250–266. https://doi.org/10.1016/j.precamres.2012.01.015.

Hölttä P. and Heilimo E. (2017) *Metamorphic Map of Finland*. Geological Survey of Finland, Special paper.

Hoskin P. W. O. and Ireland T. R. (2000) Rare earth element chemistry of zircon and its use as a provenance indicator.

Geology **28**, 627–630. https://doi.org/10.1130/0091-7613(2000)28<627:REECOZ>2.0.CO;2.

Hoskin P. W. O., Kinny P. D., Wyborn D. and Chappell B. W. (2000) Identifying Accessory Mineral Saturation during Differentiation in Granitoid Magmas: an Integrated Approach. *J Petrol* **41**, 1365–1396. https://doi.org/10.1093/petrology/41.9.1365.

Hoskin P. W. O. and Schaltegger U. (2003) The composition of zircon and igneous and metamorphic petrogenesis. *Rev. Mineral Geochem.* **53**, 27 LP-62.

Hyppönen V. (1983) *Ontojoen, Hiisijärven ja Kuhmon karttaalueiden kallioperä. [in Finnish] Summary in English: Pre-Quaternary rocks of the Ontojoki, Hiisijärvi and Kuhmo mapsheet areas. Geological map of Finland 1:100 000. Explanation to the maps of Pre-Quaternary rocks*.

Jennings E. S., Marschall H. R., Hawkesworth C. J. and Storey C. D. (2011) Characterization of magma from inclusions in zircon: apatite and biotite work well, feldspar less so. *Geology* **39**, 863–866. https://doi.org/10.1130/G32037.1.

Kemp A. I. S., Hawkesworth C. J., Foster G. L., Paterson B. A., Woodhead J. D., Hergt J. M., Gray C. M. and Whitehouse M. J. (2007) Magmatic and crustal differentiation history of granitic rocks from Hf-O isotopes in zircon. *Science* **315** (5814), 980–983. https://doi.org/10.1126/science:1136154.

King E. M., Valley J. W., Davis D. W. and Kowallis B. J. (2001) Empirical determination of oxygen isotope fractionation factors for titanite with respect to zircon and quartz. *Geochim. Cosmochim. Acta* **65**, 3165–3175. https://doi.org/10.1016/S0016-7037(01)00639-1.

Kita N. T., Ushikubo T., Fu B. and Valley J. W. (2009) High precision SIMS oxygen isotope analysis and the effect of sample topography. *Chem. Geol.* **264**, 43–57. https://doi.org/10.1016/j.chemgeo.2009.02.012.

Laurent O., Martin H., Moyen J. F. and Doucelance R. (2014) The diversity and evolution of late-Archean granitoids: evidence for the onset of "modern-style" plate tectonics between 3.0 and 2.5 Ga. *Lithos* **205**, 208–235. https://doi.org/10.1016/j.lithos.2014.06.012.

Li H. and Hermann J. (2017) The e ff ect of fl uorine and chlorine on trace element partitioning between apatite and sediment melt at subduction zone conditions. *Chem. Geol.* **473**, 55–73. https://doi.org/10.1016/j.chemgeo.2017.10.016.

Martin H., Smithies R. H. and Rapp R., et al. (2005) An overview of adakite, tonalite-trondhjemiten-granodiorite (TTG), and sanukitoid: relationships and some implications for crustal evolution. *Lithos* **79**, 1–24. https://doi.org/10.1016/j.lithos.2004.04.048.

Mcleod G. W., Dempster T. J. and Faithfull J. W. (2011) Deciphering magma-mixing processes using zonedtitanite from the Ross of Mull Granite, Scotland. *J. Petrol.* **52**, 55–82. https://doi.org/10.1093/petrology/egq071.

Miles A. J., Graham C. M. and Hawkesworth C. J., et al. (2014) Apatite: a new redox proxy for silicic magmas? *Geochim. Cosmochim. Acta* **132**, 101–119. https://doi.org/10.1016/j.gca.2014.01.040.

Power G. M., Brewer T. S., Brown M. and Gibbons W. (1990) Late Precambrian foliated plutonic complexes of the Channel Islands and La Hague: early Cadomian plutonism. *Geol. Soc. Lond.* **51**, 215–229. https://doi.org/10.1144/GSL.SP.1990.051.01.13.

Prowatke S. and Klemme S. (2005) Effect of melt composition on the partitioning of trace elements between titanite and silicate melt. *Geochim. Cosmochim. Acta* **69**, 695–709. https://doi.org/10.1016/j.gca.2004.06.037.

Prowatke S. and Klemme S. (2006a) Rare earth element partitioning between titanite and silicate melts: Henry's law revisited. *Geochim. Cosmochim. Acta* **70**, 4997–5012. https://doi.org/10.1016/j.gca.2006.07.016.

Prowatke S. and Klemme S. (2006b) Trace element partitioning between apatite and silicate melts. *Geochim. Cosmochim. Acta* **70**, 4513–4527. https://doi.org/10.1016/j.gca.2006.06.162.

Samson S. D. and D'Lemos R. S. (1999) A precise late Neoproterozoic U-Pb zircon age for the syntectonic Perelle quartz diorite, Guernsey, Channel Islands, UK. *J. Geol. Soc. Lond.* **156** (1), 47–54. https://doi.org/10.1144/gsjgs.156.1.0047.

Samson S. D., D'Lemos R. S., Blichert-Toft J. and Vervoort J. (2003) U-Pb geochronology and Hf-Nd isotope compositions of the oldest Neoproterozoic crust within the Cadomian orogen: new evidence for a unique juvenile terrane. *Earth Planet. Sci. Lett.* **208**, 165–180. https://doi.org/10.1016/S0012-821X(03)00045-1.

Stepanov A. S., Hermann J., Rubatto D. and Rapp R. P. (2012) Experimental study of monazite/melt partitioning with implications for the REE, Th and U geochemistry of crustal rocks. *Chem. Geol.* **300–301**, 200–220. https://doi.org/10.1016/j.chemgeo.2012.01.007.

Storey C. D., Smith M. P. and Jeffries T. E. (2007) In situ LA-ICP-MS U-Pb dating of metavolcanics of Norrbotten, Sweden: records of extended geological histories in complex titanite grains. *Chem. Geol.* **240**, 163–181. https://doi.org/10.1016/j.chemgeo.2007.02.004.

Sun Y., Wiedenbeck M. and Joachimski M. M., et al. (2016) Chemical and oxygen isotope composition of gem-quality apatites: Implications for oxygen isotope reference materials for secondary ion mass spectrometry (SIMS). *Chem. Geol.* **440**, 164–178. https://doi.org/10.1016/j.chemgeo.2016.07.013.

Tepper J. H. and Kuehner S. M. (1999) Complex zoning in apatite from the Idaho batholith: a record of magma mixing and intracrystalline trace element diffusion. *Am. Mineral.* **84**, 581–595. https://doi.org/10.2138/am-1999-0412.

Topley C. G., Brown M. and D'Lemos R. S., et al. (1990) The northern igneous complex of Guernsey, Channel Islands. *Geol. Soc. Lond.* **51**, 245–259. https://doi.org/10.1144/GSL.SP.1990.051.01.15.

Trotter J. A., Williams I. S., Barnes C. R., Lecuyer C. and Nicoll R. S. (2008) Did cooling oceans trigger ordovician biodiversification? Evidence from conodont thermometry. *Science* **321** (5888), 550–554. https://doi.org/10.1126/science:1155814.

Valley J. W. (2003) Oxygen isotopes in zircon. *Rev. Mineral Geochem.* **53**, 343–380.

Valley J. W., Bindeman I. N. and Peck W. H. (2003) Empirical calibration of oxygen isotope fractionation in zircon. *Geochim. Cosmochim. Acta* **67**, 3257–3266. https://doi.org/10.1016/S0016-7037(00)00090-5.

Valley J. W., Lackey J. S. and Cavosie A. J., et al. (2005) 4.4 billion years of crustal maturation: oxygen isotope ratios of magmatic zircon. *Contrib. Mineral Petrol.* **150**, 561–580. https://doi.org/10.1007/s00410-005-0025-8.

Watson E. B. and Liang Ya (1995) A simple model for sector zoning in slowly grown crystals: implications for growth rate and lattice diffusion, with emphasis on accessory minerals in crustal rocks. *Am. Mineral* **80**, 1179–1187.

Whitney D. L. and Evans B. W. (2010) Abbreviations for names of rock-forming minerals. *Am. Mineral.* **95**, 185–187. https://doi.org/10.2138/am.2010.3371.

Wilde S. A., Valley J. W., Peck W. H. and Graham C. M. (2001) Evidence from detrital zircons for the existence of continental crust and oceans on the Earth 4.4[thinsp]Gyr ago. *Nature* **409**, 175–178.

Zhang X. Y., Cherniak D. J. and Watson E. B. (2006) Oxygen diffusion in titanite: Lattice diffusion and fast-path diffusion in

single crystals. *Chem. Geol.* **235**, 105–123. https://doi.org/10.1016/j.chemgeo.2006.06.005.

Zheng Y. (1993) Calculation of oxygen isotope fractionation in anhydrous silicate minerals. *Geochimica et Cosmochimica* **57**, 1079–1091.

Zirner A. L. K., Marks M. A. W. and Wenzel T., et al. (2015) Rare earth elements in apatite as a monitor of magmatic and metasomatic processes: the Il??maussaq complex, South Greenland. *Lithos* **228–229**, 12–22. https://doi.org/10.1016/j.lithos.2015.04.013.

Associate editor: Alexander Nemchin